Soft Matter

Dynamics of the sub-ambient gelation and shearing of solutions of P3HT and P3HT blends towards active layer formation in bulk heterojunction organic solar cells

Journal:	*Soft Matter*
Manuscript ID	SM-ART-10-2020-001759.R1
Article Type:	Paper
Date Submitted by the Author:	25-Nov-2020
Complete List of Authors:	Quan , Li; Stevens Institute of Technology, Chemical Engineering Lee, Stephanie; Stevens Institute of Technology, Chemical Engineering and Materials Science Kalyon, Dilhan; Stevens Institute of Technology, Chemical Engineering

ARTICLE

Dynamics of the sub-ambient gelation and shearing of solutions of P3HT and P3HT blends towards active layer formation in bulk heterojunction organic solar cells

Received 00th January 20xx,
Accepted 00th January 20xx

DOI: 10.1039/x0xx00000x

Li Quan, Stephanie S. Lee and Dilhan M. Kalyon

Organic solar cells (OSCs) containing an active layer consisting of a nanostructured blend of a conjugated polymer like poly(3-hexylthiophene) (P3HT) and an electron acceptor have the potential of competing against silicon-based photovoltaic panels. However, this potential is largely unfulfilled first due to interrelated production and stability issues of organic solar cells and second due to the unscalable nature of the generally employed spin coating process used for the fabrication of organic solar cells. Furthermore, alternatives to spin coating, especially relying on continuous polymer processing methods like extrusion and coating, cannot be readily applied due to the typically low shear viscosity and elasticity of polymer solutions making up the active layer. Recently, He *et al.* have reported that the gelation of P3HT with [6,6]-phenyl-C61-butyric acid methyl ester ($PC_{60}BM$) under sub-ambient conditions can provide a new route to the processing of the active layers of bulk heterojunction solar cells. Furthermore, increases in power conversion efficiencies (PCEs) of the P3HT/$PC_{60}BM$ active layer were determined to be possible under certain shearing and thermal histories of the P3HT/$PC_{60}BM$ gels. Here oscillatory and steady torsional flows were used to investigate the gel formation dynamics of P3HT with a recently proposed non-fullerene acceptor o-IDTBR under sub-ambient conditions and compared with the gelation behavior of P3HT/$PC_{60}BM$ blends. The rheological material functions as well as the gel strengths defined on the basis of linear viscoelastic material functions, characterized via small-amplitude oscillatory shearing, were observed to be functions of the P3HT and o-IDTBR concentrations, the solvent used and the shearing conditions. Overall, the P3HT gels which formed upon quenching to sub-zero temperatures were found to be stable during small-amplitude oscillatory shear (linear viscoelastic range) but broke down even at the relatively low shear rates associated with steady torsional flows, suggesting that the shearing conditions used during the processing of gels of P3HT and blends of P3HT with small molecule acceptors can alter the gel structure, possibly leading to changes in the resulting active layer performance.

1 Introduction

Organic solar cells in theory represent serious potential alternatives to silicon-based solar panels that are widely employed worldwide.[1] OSCs can incorporate semiconducting layers laid on top of each other, i.e., bilayer structures[2-5] or bulk heterojunction (BHJ) active layers, i.e., nanostructured mixtures consisting of conjugated polymers (donors) and electronegative molecules (acceptors).[6-9]

For BHJ solar cells the most widely investigated donor polymer is P3HT, which is a polythiophene with a hexyl group ($(C_{10}H_{14}S)_n$.[10-14] Several different methods are reported for synthesis of highly regioregular P3HT, RR-P3HT.[15-19] P3HT with regioregular structure can aggregate and crystallize via π (also called π-π stacking) interactions.[20-25]

Chemical Engineering and Materials Science, Stevens Institute of Technology, Castle Point St., Hoboken, NJ, 07030, USA. E-mail: dkalyon@stevens.edu
Electronic Supplementary Information (ESI) is available.

During the solution-based fabrication of solar cells under ambient temperature conditions, RR-P3HT is dissolved in various solvents,[26] and when dissolved, RR-P3HT can crystallize to form colloidal particles in the form of nanowhiskers. The percolation of the nanowhiskers via interactions with each other leads to the formation of volume-spanning networks. Such networks give rise to gelation, i.e., the formation of microgels, with junction points comprised of interacting crystals.[27]

The typical organic electron acceptor molecules include $PC_{60}BM$,[28] $PC_{71}BM$,[29] and perylene diimides (PDI).[30,31] In early investigations, the efficiencies of the P3HT/$PC_{60}BM$ solar cell systems were around 2.5%.[32,33] The power efficiencies could be increased to 3.5% by 2003,[34] and to 5% by 2005.[35,36] More recently, the PCEs of devices based on P3HT/$PC_{60}BM$ blends could be increased up to 11% upon doping with low concentrations of iron (II, III) oxide nano-particles (Fe_3O_4).[37]

The fullerene acceptors used in BHJ devices, including $PC_{60}BM$, can be replaced with non-fullerene electron acceptors with PCEs of 15% and over.[38,39] The optimizations of device structures and film morphologies are essential to achieve such high PCEs. New non-fullerene acceptors, for example, rhodamine-benzothiadiazole-coupled indacenodithiophene, like, ((5Z,5′Z)-5,5′-(((4,4,9,9-tetraoctyl-4,9-dihydro-s-indaceno[1,2-

b:5,6-b′]-dithiophene2,7diyl)bis(benzo[c][1,2,5]thiadiazole-7,4-diyl))bis(methanylylidene))bis(3-ethyl-2-thioxothiazolidin-4-one)) (o-IDTBR) have also been proposed.[11,40-48] The PCE window of the P3HT/o-IDTBR system was found to be in the range of 6.4 % to 7.8%.[11,41,44,45] Overall, what made the P3HT/o-IDTBR system very interesting was the observed enhancement of the stability of the solar devices manufactured with this donor/acceptor combination.

The typical solution processing method used in fabricating the active layer of the BHJ solar cells is spin coating. However, spin coating is a batch process and is thus difficult to scale up. Alternatives to spin coating can be considered on the basis of various conventional continuous polymer mixing and film-forming processing techniques such as extrusion followed by a coating method, including doctor blading, casting, slot-die coating, gravure coating, knife-over-edge coating, off-set coating, and spray coating. Printing techniques such as ink jet printing, pad printing and screen printing are also possible.[49] However, the shear viscosity and elasticity of the polymer electron donor/organic acceptor blend solutions under the generally used ambient temperature conditions are not conducive, i.e., are too low, for the application of conventional polymer processing methods. For example, if the rheological behavior of the blend were to be suitable, twin screw extrusion and coating could have been used to first intimately blend the polymer phase with the electron acceptor and solvents in an extruder [see the Supplemental File]. Such intimate mixing processes were demonstrated for many blends of complex fluids whereby the goodness of the mixing of the ingredients, mixing indices,[50-52] could be controlled through the manipulation of the thermo-mechanical history imposed during extrusion,[50,51] enabled via mathematical modeling to optimize twin screw extrusion geometries and conditions.[53-56] Following extrusion, various coating processes can be applied.[57]

Thus, if the low viscosity and elasticity problem of the blends can be overcome, there is great potential for the use of relatively cheap and scalable extrusion/coating-based methods for the fabrication of the active layers of bulk heterojunction solar cells. Recently, He *et al.*[58] have demonstrated the sub-ambient gelation of P3HT blends involving the formation of crystalline networks via viscoelastic phase separation (VPS)[59-61] upon the quenching of P3HT solutions. The key to viscoelastic phase separation is the asymmetry in molecular dynamics between the two components of the solution.[59] In a polymer solution, the polymer phase relaxes much more slowly in comparison to the surrounding solvent molecules. More explicitly, the slow relaxing fluid component (polymers) cannot catch up with the fast relaxation of the viscous solvent during deformation. This "viscoelastic phase separation" followed by crystallization of P3HT has suggested a new route for a promising and scalable method to achieve optimized morphologies in the active layers of P3HT/$PC_{60}BM$ based organic solar cells.[58] He *et al.* indicated that: "… upon rapid cooling, viscoelastic phase separation occurring in electron-donating RR-P3HT solutions leads to the formation of stable, crystalline RR-P3HT gel networks with hierarchical porosity that improve the light harvesting efficiency of solar cell active layers".[58] This crystallization-induced gelation during VPS was found to be thermo-reversible and insensitive to the presence of both $PC_{60}BM$ and noncrystallizing regio-random P3HT, Rra-P3HT.[58] It was proposed that once formed in solution, the semicrystalline RR-P3HT networks can be transferred to OSC device platforms via continuous processing including extrusion and doctor blading. It was revealed that OSCs comprising cooled photoactive layers displayed 45% higher efficiencies compared to those comprising uncooled photoactive layers.[58]

The objective of the current investigation is to build upon the earlier investigation of He *et al.* by characterizing the sub-ambient gel formation behavior of P3HT blended with o-IDTBR, i.e., another popular small molecule acceptor as described earlier. Two different solvents were used, and the data were collected as a function of the concentrations of P3HT and o-IDTBR. Rheological analysis was employed as a tool to compare the gel formation dynamics and gel strengths of P3HT with o-IDTBR, with those of P3HT and $PC_{60}BM$ blends. As noted, Holliday *et al.* have shown that the o-IDTBR acceptor has significant advantages over the conventional $PC_{60}BM$ acceptors due to the improved shelf-life and photo-oxidation stability of the P3HT/o-IDTBR system in comparison to the conventional P3HT/$PC_{60}BM$.[11]

2 Experimental

2.1 Materials

In this investigation we have used only RR-P3HT. Thus, all subsequent references to P3HT should be taken to mean RR-P3HT. P3HT was purchased from Rieke Metals (Lincoln, NE), with weight-average molecular weight of 50−70 kDa and regioregularity=91% (the degree of regioregularity was measured through the number of head-to-tail linkages in the polymer). o-IDTBR was procured from Derthon, Inc. (Shenzhen, CN) with purity>99% and Mw=1326 g/mol. The solvents 1,2-dichlorobenzene (o-DCB) and o-xylene (purity≥99%) were received from Sigma-Aldrich. All materials were used as received without further purification. Information on experimental equipment, methods and procedures are available in the supplemental files and summaries are provided next.

2.2 Sample Preparation

Sample solutions were prepared by dissolving pure P3HT and blends of P3HT/o-IDTBR in o-DCB or o-xylene on top of a hot plate under magnetic stirring condition. The rotational speed of the magnet was set at 500 rpm and the dissolution temperature was 70 °C. Typically, the dissolution took about 2-3 hours. Total concentrations of P3HT in the solvent were varied between 6.25 to 25 mg of P3HT per ml of solvent, i.e., mg/ml. Solutions of blends of P3HT and o-IDTBR were prepared at the P3HT over o-IDTBR weight ratios of 1:1, 1:1.6 and 1:2.

2.3 Small-amplitude oscillatory flow

During oscillatory shearing, the shear strain, γ, varies sinusoidally with time, t, at a frequency of ω, i.e., $\gamma(t) = \gamma^0 sin(\omega t)$, where γ^0 is the strain amplitude. The shear stress, $\tau(t)$, response

of the fluid to the imposed deformation consists of two contributions associated with the energy stored as elastic energy and energy dissipated as heat, i.e., $\tau(t) = G'(\omega)\gamma^0 sin(\omega t)+G''(\omega)\gamma^0 cos(\omega t)$, where the first part on the right of the equation is associated with the elastic energy storage and the second part is associated with dissipation. The two moduli, i.e., the storage modulus, G', and the loss modulus G'', are characterized as a function of the strain amplitude, γ^0, and then frequency, ω. In the linear viscoelastic region, all dynamic properties are independent of the strain amplitude, γ^0, thus strain amplitude scans were applied first to assure that the dynamic properties could be determined under linear viscoelastic conditions. The use of multiple frequencies, ω, during oscillatory shearing provides the ability to fingerprint the characteristic time dependence of the linear viscoelastic properties. Considering that the Deborah number is the ratio of the relaxation time of the fluid over the characteristic time for the deformation, such frequency dependent experiments provide data over a broad range of Deborah numbers. Overall, two types of sinusoidal experiments were carried out in oscillatory shearing, i.e., time sweeps during which the frequency and the strain amplitude were kept constant upon reaching −5 °C and frequency sweeps that were imposed when asymptotic behavior was observed from the time sweeps carried out at −5 °C.

In order to capture the sol-gel transition kinetics, oscillatory shear data were collected first as a function of time at constant γ^0 and ω. Time sweep tests were continued until the ultimate plateau values for G' and G'' are reached (whereby constant G' and G'' could be sustained for durations longer than 10 min). The achievement of the plateau region for dynamic properties indicates that the gel that was formed has achieved a steady-state structure, and that the solvent loss is negligible. Upon reaching the plateau region, the linear viscoelastic material functions, G' and G'', were collected as a function of frequency, ω at a constant γ^0. As noted earlier at the linear viscoelastic region the moduli are independent of the strain amplitude, γ^0.

2.4 Steady torsional flow

Steady torsional experiments were carried out in attempt to characterize the development of the shear viscosity of the solution samples upon the imposed thermal treatment (exposure to −5 °C). These experiments were carried out using parallel plate fixtures employing multiple gaps. Multiple gaps are recommended to be used for complex fluids, including microgels and concentrated suspensions to be able to characterize the wall slip versus the shear stress relationship and to enable the determination of the true shear rates that are imposed.[62-66]

2.5 Differential scanning calorimetry (DSC) experiments

DSC experiments were carried out using a TA Instrument DSCQ100 at a heating rate of 5 °C/min under nitrogen. Samples were prepared by placing solutions into the ARES chamber at −5 °C for 5 min and then drop casting the solutions onto glass substrates. The solvent was then allowed to evaporate in a nitrogen glove box for 48 hr. After the solvent being completely evaporated, the dried film was transferred into DSC pans, constructed out of aluminum. No pre-shearing was applied, thus the rheometer was only used as a thermal treatment apparatus prior to the removal of the solvent under ambient temperature conditions (23±2 °C).

3 Results and discussion

The first set of figures, i.e., Fig. 1-3 show the dynamic properties of pure P3HT solutions at −5 °C. In these experiments P3HT solutions were cooled from room temperature to −5 °C and kept at −5 °C while subjecting the solution samples to small-amplitude oscillatory shear and recording the dynamic properties as a function of time. These time scans were then followed by frequency scans as explained below.

Fig. 1 shows the time dependencies of the G' values of P3HT solutions in o-DCB at two P3HT concentrations of 12.5 and 25 mg/ml. These samples were quenched to −5 °C and the oscillatory shear was imposed at a frequency of 1 radians/s (rps) and a strain amplitude of 1% at the edge. At the P3HT concentration of 12.5 mg/ml the storage modulus grew slowly to reach a plateau value, i.e., about 800 Pa after about 3600 s. The 95% confidence intervals determined according to Student's t-distribution are presented and the confidence intervals are rather broad. The increase of the P3HT concentration to 25 mg/ml gave rise to an accelerated growth of the storage modulus which reached to a plateau of around 10 kPa within about 1500 s. The slope dG'/dt (shown in the inset of Fig. 1) increases up to a maximum at 620 s and then decreases to zero after 1500 s at which the plateau region is reached.

At the plateau region the elastic moduli no longer changed with additional time of oscillatory shearing. The time to reach the plateau decreased with increasing concentration of P3HT, i.e., from a duration of 3600 s at 12.5 mg/ml to 1500 s at 25 mg/ml. The G' value at the plateau, denoted as G'_{max}, depended on the concentration of the P3HT, with the value of G'_{max} increasing from 800 Pa to 10^4 Pa as the P3HT concentration in o-DCB was increased from 12.5 to 25 mg/ml. The two picture insets of Fig. 1 show that the solutions were free flowing at room

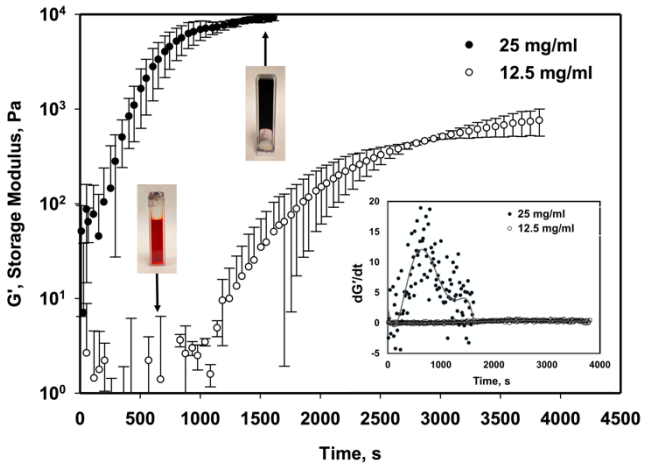

Figure 1. Storage modulus, G', versus time, t, of P3HT in o-DCB at two concentrations following rapid cooling to -5 °C. The insets are pictures showing the free-flowing nature of P3HT solutions at -5 °C prior to gelation and upon gelation. A plot of dG'/dt versus time is also included for the two concentrations of P3HT.

temperature with a bright red color and became solid-like upon reaching the plateau behavior with a dark brown color.

Fig. 2 shows the dependency of the storage moduli, G', on the frequency of oscillation in the plateau region for six concentrations of P3HT. These frequency sweeps were carried out following the reaching of the plateau behavior during time sweeps at 1 rps for 1000 s. The typical 95% confidence intervals determined according to Student's t-distribution are reported in Fig. 2. The confidence intervals obtained from three successive runs are relatively narrow indicating that the structures achieved during different runs at −5 °C were very reproducible to give rise to similar elastic behavior, as reflected in the narrow ranges of G' obtained. It appears that the dynamic properties characterized in the linear viscoelastic range are stable to changes in frequency and time ranges associated with the relatively modest strains and strain rates of the linear viscoelastic range, indicating that the gels which form conserve their structures during subsequent oscillatory shearing in the linear range.

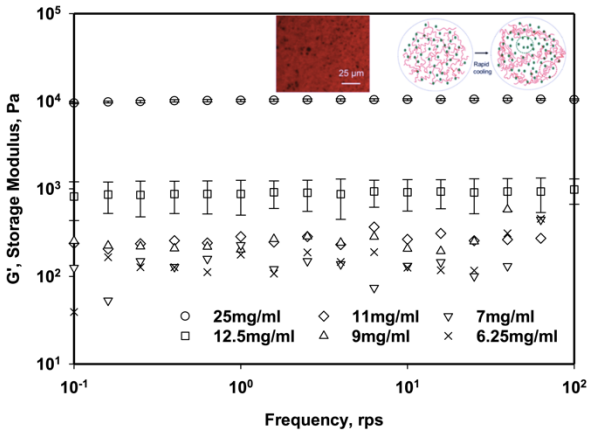

Figure 2. Storage modulus, G', versus frequency, ω, of P3HT solutions in o-DCB with concentrations of 6.25, 7, 9, 11, 12.5, and 25 mg/ml at −5 °C. The insets are the confocal fluorescence micrograph and schematic representation of cooling-induced viscoelastic phase separation process of P3HT solution[58].

In the six sets of experiments reported in Fig. 2, the concentration of the P3HT was varied between 6.25 to 25 mg/ml. At all concentrations, the storage moduli were independent of the frequency in the plateau region. Such independence of the dynamic properties from the frequency of oscillation in oscillatory shearing is one of the traits of "gel-like" behavior.[67] With increasing concentration of the P3HT the storage modulus values increase from 170 Pa at 6.25 mg/ml to about 800 Pa at 12.5 mg/ml. The frequency-independent storage modulus values represent the "gel strength" of the quenched P3HT in o-DCB samples. As shown in Fig. 2 the concentration of P3HT makes little difference on the gel strength in the concentration range of 6.25 to 11 mg/ml, with the storage moduli falling in the 170-270 Pa range. However, the concentration of the P3HT makes a significant difference in the storage modulus values, representing the gel strengths, when the concentration of P3HT was increased further. Going from 12.5 mg/ml to 25 mg/ml the storage modulus values increased from 800 to 10^4 Pa. This behavior is consistent with the results of the earlier investigation of He *et al.* Their results indicated that when the concentration of P3HT in o-DCB was increased from 12.5 to 50 mg/ml the storage modulus of the gel increased from 1 to 50 kPa.[58]

The inset in Fig. 2 shows a typical confocal fluorescence micrograph of cooled solutions of P3HT.[58] The cooling-induced structural rearrangements were associated with a viscoelastic phase separation process followed by crystallization in conjunction with the formation of a network of nanowhisker-shaped crystallites.[68] The confocal micrographs obtained by He and co-workers of P3HT cooled to −5 °C revealed micron-sized solvent-rich "holes" (indicated as the darker regions in the micrograph shown in Fig. 2) due to phase separation and interchain crystallization as depicted schematically in the inset of Fig. 2. Cryogen based scanning electron micrographs revealed further an interfibrillar network exhibiting nano sized pores.[61] Similar processes associated with interchain crystallization are also expected for P3HT and o-IDTBR blends, thus giving rise to the gelation behavior reported here.

Fig. 3a and b indicate that the G' values are more sensitive to the structure of the gel in comparison to G'', i.e., G' is dependent on the concentration of the P3HT for both the relatively small concentrations (6.25 to 12.5 mg/ml) as well as the higher concentration range of 12.5 to 25 mg/ml (Fig. 3a). Fig. 3b indicates that G'' is sensitive to the concentration of the P3HT only in the concentration range of 12.5 to 25 mg/ml. The results in Fig. 3 show that the elasticity of the gel (as represented by the values of G') is more sensitive to concentration in comparison to the dependence of the viscosity and the viscous dissipation behavior of the gel versus the concentration of P3HT (as

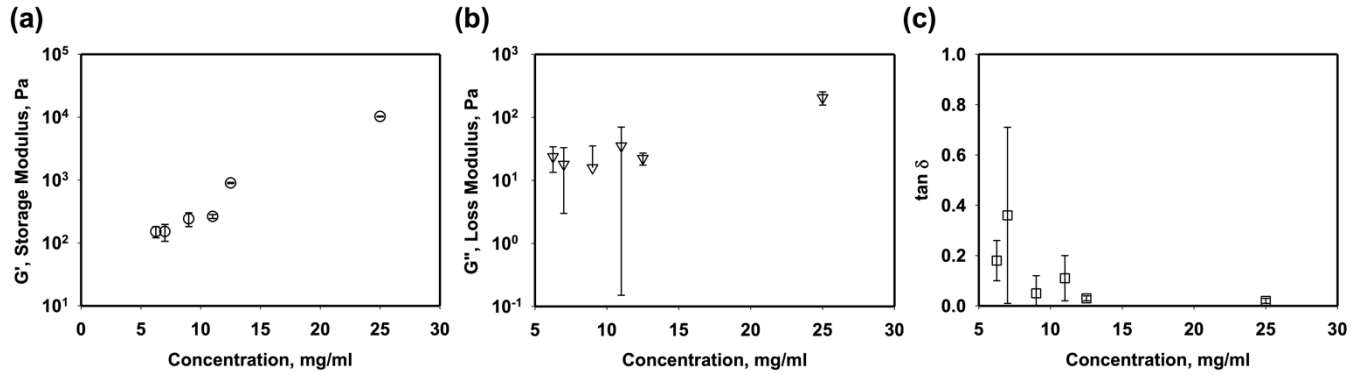

Figure 3. (a) Storage modulus, G' (b) Loss modulus, G'' (c) tan δ versus P3HT in o-DCB of concentrations of 6.25, 7, 9, 11, 12.5, and 25 mg/ml at −5 °C.

represented by the values of G''). Finally, tan $\delta = G''/G'$ values exhibit significantly broad confidence intervals and do not provide any clear-cut dependence on P3HT concentration. The fact that both G' and G'' increase with concentration may be a contributor, so that the G''/G' ratios do not vary significantly with P3HT concentration.

Fig. 4 displays both the storage moduli, G', and the loss moduli, G'', as well as the tan δ values of pure P3HT solutions as a function of frequency in the plateau region for two different solvents, o-DCB and o-xylene. The results with both solvents again point to the gel-like behavior of the solution samples of P3HT upon reaching plateau regions following time scans of small-amplitude oscillatory shearing at −5 °C. First, the loss moduli, G'', are within a narrow range of 100 to 450 Pa and are independent of frequency for both o-DCB and o-xylene. Consistent with the earlier observation that in o-DCB the storage moduli of the P3HT solutions in o-xylene are also independent of frequency, i.e., they are within a small range of 9600 to 10500 Pa. For both solvents the storage moduli are significantly higher than the loss moduli ($G' >> G''$) over the entire frequency range tested, i.e., 0.1 to 100 rps. The G' values are about 24-96 times greater than G'' values at similar frequencies. As shown in Fig. 4, the resulting values of tan $\delta = G''/G'$ are all smaller than 0.1, providing another manifestation of gel-like behavior.[67] Thus, for both solvents quenching the P3HT solution samples to −5 °C results in the formation of a gel. However, the gel strength values depend on the solvent used. Solution samples with o-DCB gave rise to significantly higher gel strengths (an order of magnitude higher G' values for o-DCB versus o-xylene) in comparison to the gel strength of P3HT solutions with o-xylene, associated with the differences in solubilities in these two solvents as explained later. The loss modulus values were not affected by the solvent type.

The next set of three figures, i.e., Fig. 5-7 show the dynamic properties of blends of P3HT with o-IDTBR. The time dependent behavior of the storage modulus for solution samples with equal amounts of P3HT and o-IDTBR (1:1 P3HT:o-IDTBR, 25 mg/ml each) dissolved in o-DCB and o-xylene when quenched to and kept at −5 °C at a constant frequency of 1 rps and a constant strain amplitude of 1% are shown in Fig. 5. Consistent with the

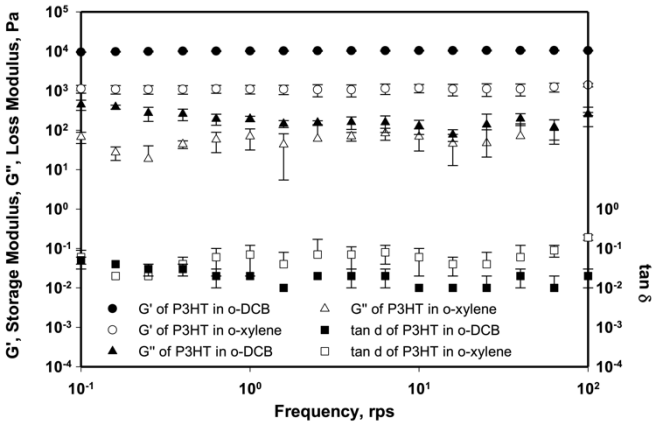

Figure 4. Storage modulus, G', loss modulus, G'', and tan δ versus frequency, ω, for 25 mg/ml P3HT in two different solvents o-DCB and o-xylene.

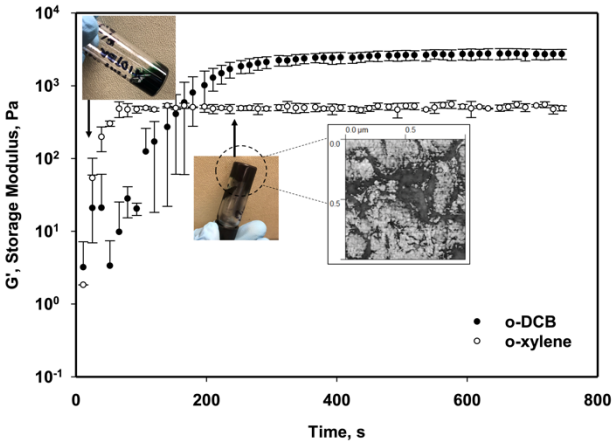

Figure 5. Storage modulus, G', versus time, t, of P3HT and o-IDTBR solutions in o-DCB and o-xylene at −5 °C. The two pictures show that the P3HT /o-IDTBR solutions are free flowing prior to gelation and solid like upon gelation. An AFM phase image of the bulk heterojunction active layer composed of the blend of P3HT/o-IDTBR is also included as an inset.

earlier observed time-dependent behavior of pure P3HT solutions at −5 °C, the storage moduli of blends of P3HT with o-IDTBR also monotonically increase to asymptotic ultimate values, i.e., reach plateau values. With increasing oscillatory shearing time at −5 °C the storage modulus, which is indicative of the elasticity of the solution increased by about three orders of magnitude for both solvents at P3HT and o-IDTBR concentration of 25 mg/ml each.

Consistent with the behavior of pure P3HT (as was shown in Fig. 1) the insets included in Fig. 5 indicate that the P3HT and o-IDTBR blend solutions were free flowing at room temperature and became solid-like upon reaching −5 °C (when the container was flipped there was no flow). The two solvents generated different time-dependent behavior. With o-DCB the storage modulus, G' is relatively low at the beginning of the time sweep, followed by a significant increase with time of oscillatory shearing to reach an asymptotic plateau, i.e., about 2200 Pa in about 1000 s. Further shearing does not change the plateau behavior. On the other hand, the 25 mg/ml each P3HT and o-IDTBR solution in o-xylene exhibited a relatively high G' within about 120 s when the temperature was reduced to −5 °C and overall reached its plateau value significantly faster than the P3HT and o-IDTBR blend dissolved in o-DCB solvent. Fig. 5 also shows a phase image obtained with atomic force microscopy (AFM) (captured after the solvent o-DCB was evaporated) of the bulk heterojunction active layer composed of the blend of P3HT with o-IDTBR. The nanostructured nature of the morphology of the blend constituting the active layer is indicated, i.e., the domain sizes are in the 200 nm range. The observed large phase separation would result in less interfacial area between the donor and acceptor for exciton dissociation, but at the same time, larger domains are better for charge transport to the electrodes.

Fig. 6 displays the comparison of the storage modulus, G', as a function of frequency, ω, after the plateau behavior is reached at −5 °C solutions of pure P3HT and P3HT blended either with $PC_{60}BM$ or o-IDTBR in two different solvents, i.e., o-DCB or o-xylene. Both the donor and the electron acceptors were kept at a constant concentration of 25 mg/ml. In contrast to the $PC_{60}BM$

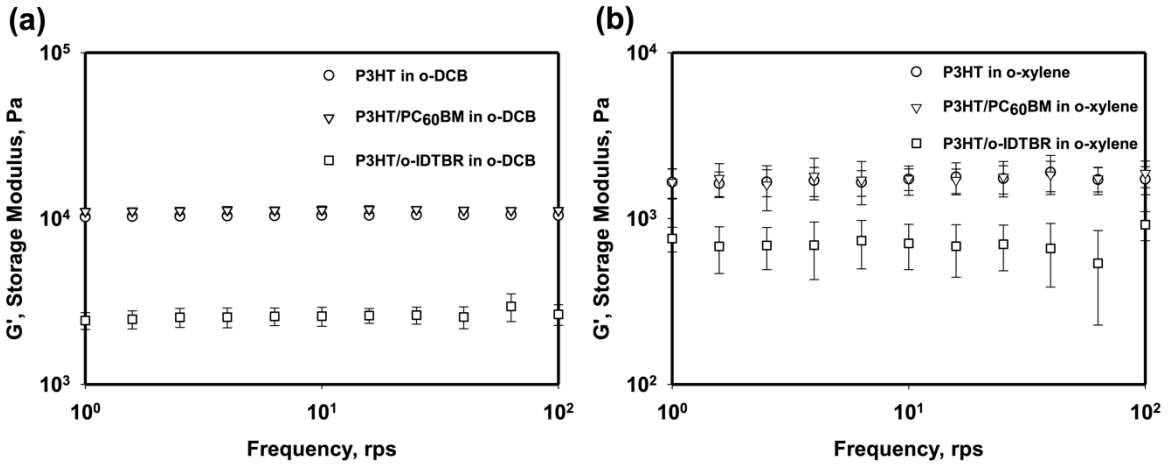

Figure 6. Storage modulus, *G′*, versus frequency, *ω*, for P3HT, P3HT/$PC_{60}BM$ and P3HT/o-IDTBR in two different solvents (a) o-DCB and (b) o-xylene, all at concentrations of 25 mg/ml.

making no difference in the gel strength of P3HT for both solvents the replacement of o-IDTBR with $PC_{60}BM$ makes a big difference on the gel strength for both o-DCB and o-xylene. As shown in Fig. 6, the gel strength of the solution is diminished when o-IDTBR is added to P3HT. The reduction of the storage modulus generated by the addition of o-IDTBR is greater for o-DCB (going from 10^4 Pa for pure P3HT to 2200 Pa for the P3HT/o-IDTBR blend) in comparison to the decrease of the storage modulus with o-xylene (from 1800 Pa for pure P3HT to 700 Pa for the P3HT/o-IDTBR blend).

Fig. 7 displays the storage modulus, *G´*, versus frequency, *ω*, of P3HT blended with o-IDTBR at different concentration ratios, i.e., 1:1 (25 mg/ml each of P3HT and o-IDTBR), 1:1.6 (25 mg/ml of P3HT and 40 mg/ml o-IDTBR) to 1:2 (25 mg/ml of P3HT and 50 mg/ml o-IDTBR) in o-DCB and o-xylene. The frequency sweeps were again carried out at −5 °C following time sweeps which resulted in reaching of the plateau behavior. Fig. 7 also shows the storage modulus values for pure P3HT at 25 mg/ml. For both concentrations of o-IDTBR blended with P3HT the solution samples exhibited gel behavior upon being cooled to −5 °C and reached a plateau in *G´*. The highest gel strengths were observed for pure P3HT solutions. As indicated earlier, adding o-IDTBR into P3HT system disrupts P3HT crystallization, thus lowering the gel strength. However, these results indicate that the concentration of o-IDTBR in the range investigated did not affect the strength of the gel which forms.

The results presented in Fig. 6 and 7 indicate that P3HT and blends of P3HT with $PC_{60}BM$ or with o-IDTBR form gels when subjected to –5 °C. When the solution is held under quiescent conditions or when subjected to small-amplitude oscillatory shearing as a function of time under constant frequency and strain amplitude the structure of the gel evolves until an equilibrium structure is achieved, which coincides with the gel strength remaining constant for longer durations. Previous investigations have shown that the gelation of P3HT when quenched can be considered to occur in two stages. In the first stage the quenching of the solution can result in "viscoelastic phase separation", as affected by the high molecular weight and the associated long relaxation times of the polymer phase, P3HT. The solvent and the electron acceptor whether $PC_{60}BM$ or o-IDTBR exhibit significantly smaller relaxation times. The differences in relaxation behavior following quenching results in the separation of the P3HT from the small molecules to some extent and leads to the formation of solvent holes.[58-60] The aggregation of the P3HT macromolecules via *π*-*π* bonding as explained earlier then leads to the crystallization of the P3HT and

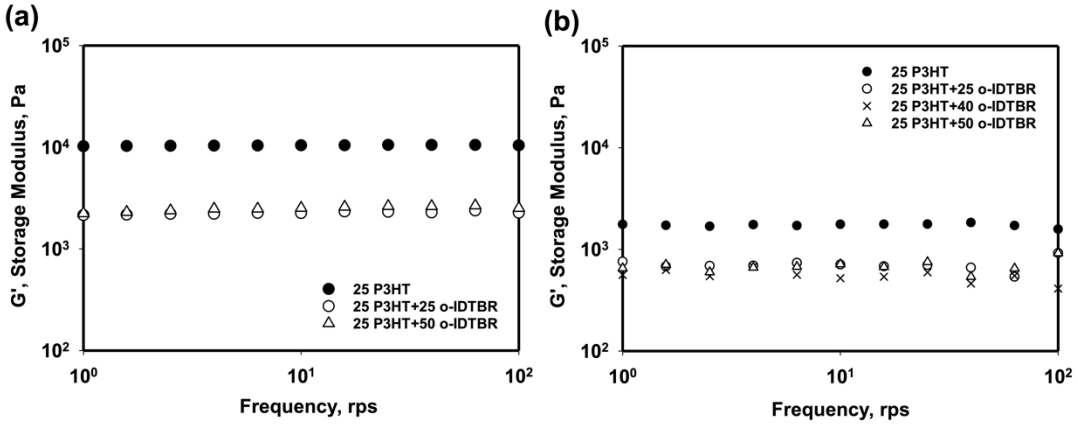

Figure 7. *G´* versus frequency, *ω*, of solutions comprising blends of P3HT and o-IDTBR (a) in o-DCB with o-IDTBR's concentrations of 0, 25 and 50 mg/ml. (b) in o-xylene with o-IDTBR's concentrations of 0, 25, 40 and 50 mg/ml.

the formation of nanowhiskers. The aggregation and the formation of the nanowhiskers generate a network that spans the volume of the sample, giving rise to solid like nature and the gel-like behavior observed via the dynamic properties ($G' >> G''$ and $G' \neq fn(\omega)$).

These results overall show that the nature of the solvent makes a difference in the dynamics of the phase separation and the strength of the gel which forms. Here we have used two solvents with different solubility parameters, i.e., o-DCB with a solubility parameter of 20.1 $MPa^{0.5}$ and o-xylene with a solubility parameter of 18.1 $MPa^{0.5}$.[69] The solubility parameter for P3HT is 19.43 $MPa^{0.5}$.[70] All the values were measured at 25 °C. The solubility parameter of o-DCB is very close to the solubility parameter of P3HT (20.1 $MPa^{0.5}$ versus 19.43 $MPa^{0.5}$, respectively). On the other hand, the solubility parameter of o-xylene is smaller than that of P3HT (18.1 $MPa^{0.5}$ versus 19.43 $MPa^{0.5}$) indicating that o-DCB is a better solvent for P3HT under ambient tempratrure conditions. The differences are also reflected in the solubility of P3HT in o-DCB and o-xylene under ambien temperature. The solubility of P3HT is 14.7 mg/ml in o-DCB, while in o-xylene is 2.7 mg/ml, indicating that o-DCB is indeed a much better solvent whereas o-xylene is a poor solvent (a theta solvent) for P3HT at ambient temperature. With a good solvent the P3HT macromolecules exhibit greater radii of gyration (the radius is indicative of the swept volume of P3HT in solvent), whereas with a poor solvent the radius of gyration is much smaller. When the radius of gyration of the macromolecule is reduced in the solution the probability of chains coming into close proximity with each other to give rise to aggregation via π-π bonds and to the crystallization of nanowhiskers to lead to a solid-like network upon the interactions of the nanowhiskers with each other is small, thus reducing the crystallinity and consequently the gel strength. The reduction of the gel strength with the poor solvent o-xylene is clearly shown in Fig. 4-6.

The electron acceptor also plays a significant role, albeit different roles for different acceptors (assuming that the relative behavior observed at ambient temperature holds at −5 °C. At −5 °C the incorporation of $PC_{60}BM$ into P3HT does not affect the gel strength.[58] On the other hand, upon blending of $PC_{60}BM$ with o-IDTBR the gel strength decreases significantly. These results suggest that o-IDTBR disrupts the aggregation and crystallization of P3HT while $PC_{60}BM$ does not, as shown in Fig. 6 and 7. The mechanism for the disruption should be associated with the intercalation of o-IDTBR into the gallery space between layers of P3HT to disrupt the aggregation and the subsequent crystallization of P3HT,[44,71] suggesting that the P3HT and o-IDTBR are more miscible in each other in comparison with P3HT and $PC_{60}BM$ at −5 °C. The mechanisms need to be investigated in subsequent studies. Collins has indicated that $PC_{60}BM$ largely migrates into the amorphous region of P3HT molecules. When the concentration of the $PC_{60}BM$ is increased beyond a critical value the extra $PC_{60}BM$ undergoes phase separation and migrates out of the vicinity of P3HT.[72]

Fig. 8 shows the results of steady torsional flow for pure P3HT solution, 25 mg/ml of P3HT in o-DCB (Fig. 8a) followed by frequency sweep tests of samples captured at different durations of steady torsional flow (Fig. 8b). The torque, $\Im$, is reported as a function of time when applying a constant apparent shear rate of 1 s^{-1} at −5 °C. The experiment involved quenching the solution to −5 °C and holding the sample under quiescent conditions at –5 °C for 660 s total. Holding the P3HT solution at −5 °C under quiescent conditions gives rise to G' values which are independent of the frequency with $G' >> G''$, i.e., the hallmarks of gel-like behavior. Fig. 8a shows the torque versus time behavior during steady torsional flow following the quiescent holding of the gel at –5 °C for 660 s.

The torque versus time result for the P3HT gel during steady torsional flow at −5 °C is very interesting and to our knowledge is being reported for the first time. During steady torsional flow one would have expected the torque (and hence the shear stress) to increase to a constant plateau value and remain there as was observed with the dynamic properties reaching plateau values during oscillatory shear flow. However, this is not what happens. The behavior includes an increase of the torque (hence the shear stress) monotonically until a maximum is reached. The maximum torque is reached at about 0.2 s of shearing. Further shearing during the next 100 s results in the torque to decrease

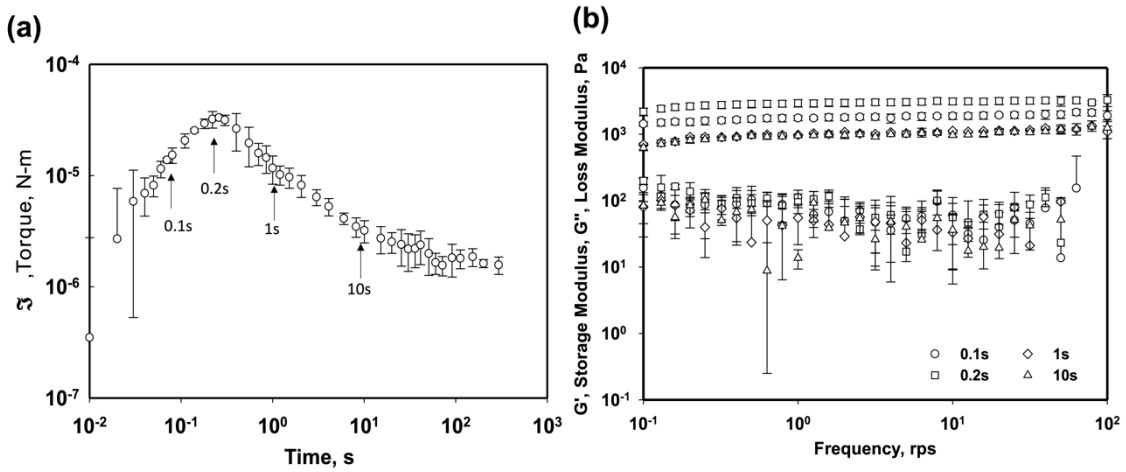

Figure 8. (a) Steady torsional flow of 25 mg/ml P3HT in o-DCB with gap of 0.4 mm at −5 °C. (b) G' versus frequency, ω, after steady torsional shearing for fixed times, 0.1 s, 0.2 s, 1 s and 10 s at −5 °C.

continuously (from a maximum of 3.5×10^{-5} N-m at 0.25 s, to 2×10^{-6} N-m at 70 s).

Such a decrease can be explained in two ways. The first explanation could be that gels being viscoplastic materials would exhibit wall slip, and the transition from no slip to wall slip can be occurring when a critical shear stress of 250 Pa (torque of 3.5×10^{-5} N-m) is reached during shearing at constant apparent shear rate.[64-66,73] The transition from no slip to wall slip have been observed also with pure polymers, i.e., pure polymer melts can exhibit critical shear stress values at which wall slip is onset. For example, silicone polymers typically start to exhibit readily noticeable wall slip when the shear stress reaches 60 kPa. On the other hand, polyethylene melts typically exhibit a critical shear stress of 200 kPa at which they start to exhibit wall slip.[57,74-78]

Another mechanism that can explain the observed differences in steady torsional flow versus small-amplitude oscillatory shearing behavior is associated with the evolution of the structure (or lack of it) in the linear versus the non-linear nature of the deformations that are imposed. The time dependent dynamic properties were obtained in the linear viscoelastic region. In the linear region the structure of the gel by definition should not change significantly since both the strain and the strain rate are relatively small, i.e., the structure is not far removed from its equilibrium state. This is predicated on the observation that in the linear region the moduli are independent of the strain amplitude as indeed observed here. On the other hand, the steady torsional flow is being carried out at a relatively high shear rate of 1 s^{-1} which is in the non-linear viscoelastic region so that changes in the structure of the gel may be expected.

A set of supporting oscillatory shearing experiments were carried out to answer the question as to whether it was the wall slip or the structure evolution that gave rise to the torque (and hence the shear stress) versus time behavior noted in Fig. 8. The dynamic properties are very sensitive to the structure of a gel. Thus, inferences on the evolution of the structure of the gel during torsional flow can be made on the basis of the characterization of the dynamic properties following steady torsional flow at constant apparent shear rate of 1 s^{-1} for different durations of time. The methodology involved quenching the sample and holding it at –5 °C for 11 minutes and then the imposition of the steady shear flow and coming to dead stops at various shearing durations, i.e., 0.1 s, 0.2 s, 1 s and 10 s after the inception of the steady shear flow. The storage and loss moduli as a function of frequency collected on samples that were subjected to shearing in steady torsional flow for different durations are shown in Fig. 8b. First, regardless of the duration of steady torsional flow all samples exhibit gel-like behavior as evidenced by the storage and the loss moduli being independent of the frequency and $G'>>G''$. Thus, the samples remain as gels regardless of the duration of torsional flow. However, the dynamic properties associated with the plateau behavior change significantly with the duration of the steady torsional flow. This indicates that the gel strength depends on the duration of the steady torsional flow that is imposed. The maximum storage modulus, i.e., the maximum gel strength, is observed at 0.2 s, at which a maximum torque is also observed (highest gel strength). The G'' values exhibit some scatter associated with their relatively small values (about 10-100 Pa) with respect to the transducer sensitivity of the rheometer.

Fig. 8a further shows that following the maximum torque, the storage modulus values decrease significantly (from 3000 Pa at 0.2 s to 1000 Pa at 10 s) as the duration of the steady torsional flow is increased. The gel strengths of solution samples sheared for 1 s are about the same as those sheared for 10 s. This indicates that the structure that was built during steady torsional flow up to the maximum shear stress was subsequently broken in such a way (step change) that additional shearing no longer made a difference on the structure. Thus, at −5 °C there is a critical shear stress for P3HT gels above which the structure of the gel is diminished. This critical shear stress is about 250 Pa (corresponding to the maximum observed torque value of 3.5×10^{-5} N-m in Fig. 8a).

Overall, these results indicate that the solutions of P3HT or P3HT blends with electron acceptors become gel-like at –5 °C with the gel strength depending on the duration of time that the sample is held under quiescent conditions or under small amplitude oscillatory shearing conditions until a plateau is reached. When this gel is further sheared using steady torsional flow (shearing in the non-linear region) the structure of the gel is altered in such a way that the gel-like behavior prevails but the gel strength is reduced upon shearing beyond the critical shear stress (as indicated by decrease of the storage modulus).

What is the role of wall slip in the observed steady torsional flow behavior? As indicated earlier, for some complex fluids, including polymer melts, wall slip can be onset at a critical shear stress, with the value of the critical shear stress depending on the nature of the polymer melt. This is elucidated next in Fig. 9.

Fig. 9 shows the steady torsional flow experiments that were carried out on fresh solutions of 25 mg/ml P3HT in o-DCB at −5 °C, following the procedures outlined for the results reported in Fig. 8 but collected using three different gaps, which were 0.4, 0.8 and 1.2 mm. Thus, for each gap the samples were quenched to –5 °C, held there for 11 min and then the steady torsional flow was initiated at an apparent shear rate of 1 s^{-1}. The overall torque (or shear stress) versus time behavior at −5 °C was similar for the three gaps. The torque went up to a maximum, $\mathfrak{I}_{max,}$ and then

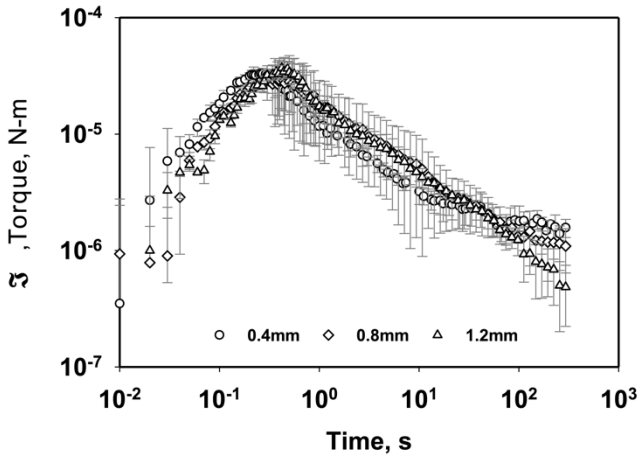

Figure 9. Steady-torsional tests torque, $\mathfrak{I}$, versus time, t, of 25 mg/ml P3HT solutions in o-DCB with gaps varying from 0.4, 0.8, and 1.2 mm at −5 °C.

decreased monotonically with continued shearing. The $\Im_{max}$ of these three gaps remained largely unchanged, i.e., in the 3.5×10^{-5} N-m to 4.0×10^{-5} N-m range. This result indicates that although the value of the maximum torque did not change significantly, the time to reach the maximum torque somewhat increased with the increasing gap values.

The relatively broad confidence intervals noted precluded any inferences to be made on the effects of the surface to volume ratio of the geometry within which the solution samples are sheared. Generally, with wall slip the shear stress (and hence the torque) decreases with increasing surface to volume ratio (proportional to reciprocal gap). Thus, the true nature of the contribution of wall slip to the observed steady torsional flow behavior could not be made.

Fig. 10 reports the time dependence of the torque (shearing stress) at different apparent shear rates for a blend of P3HT with $PC_{60}BM$ at concentrations of 25 mg/ml with a ratio of 1:1 in o-DCB. Similar results are shown in Fig. S11 of the Supplemental file on pure P3HT solution at various apparent shear rates. Fig. 10 indicates that the nanocrystalline structure is disrupted at a torque of 4×10^{-5} N-m to 7.5×10^{-5} N-m regardless of the apparent shear rate (the corresponding critical shear stress at the edge of the specimen is 400-750 Pa). Furthermore, the structure deterioration (disruption of the crystalline order) as evidenced by the decreases of the torque and hence the shear stress continue with the torque/shear stress decreasing monotonically with time (and hence with increasing total strain) for all apparent shear rates except the lowest apparent shear rate of 0.001 s^{-1}. For this apparent shear rate the torque remains constant. This leveling off with time at the apparent shear rate of 0.001 s^{-1} is very likely a result of plug flow formation and wall slip, since it is indeed expected that the shear stress will be reduced with increasing strain on the gel. The reduction of the duration that the apparent shear rate is applied (and hence the reduction of the total strain imposed during processing) can lead to better-preserved crystalline structure during film formation.

Fig. 10 also suggests that the type of deformation that is imposed during film formation can lead to very significant heterogeneities in the films that are deposited. For example, if a slot die is used (Poiseuille flow) the shear rate would be a maximum at the wall and zero at the plane of symmetry. Thus, the crystalline order would be significantly deteriorated at the wall due to the high shear rates (and hence highest strains) that are applied, whereas the crystalline structure would be undisturbed at the plane of symmetry. Significant differences in imposed shear rates and total strains across the gel thickness during film formation would give rise to heterogeneous active layers, with different layers exhibiting different structures and gel strengths. Processing flows based on pure drag flow (gelled solution is sandwiched in between two plates one of which is moving and the other is stationary) that generate a linear velocity distribution in the flow channel and hence a constant shear rate, are preferable for the conservation of networks from aggregated and crystallized P3HT. The role of the residence time in the film forming geometry is also important. The smaller the mean residence time, the smaller is the strain imposed on the gel leading to better preservation of the crystalline structure.

These results further point to the importance of the wall boundary condition during coating.[79] Wall treatments that increase the wall slip velocity and hence lower the shear rate on the gel during processing would be preferable.

DSC measurements were carried out on solutions of blends of P3HT with o-IDTBR first exposed to −5 °C and then drop-cast under ambient temperature conditions in a glove box. During DSC experiments under N_2 the temperature was increased from 40 °C to 300 °C at 5 °C/min (first heating) followed by cooling to 0 °C and then increased to 300 °C again (second heating). The procedure allowed samples to have a consistent thermal history prior to the characterization of their degree of crystallinity. Fig. 11 shows that there are significant differences in the thermal behavior of P3HT versus P3HT blended with o-IDTBR.

During the second heating P3HT/o-IDTBR blend undergoes an exothermic crystallization transition with an onset temperature of 105 °C and a crystallization peak temperature of 117 °C (first peak). With increasing temperature, the crystallites melt starting at a temperature of about around 188 °C and the melting is completed at a temperature of 230 °C. Thus, 230 °C is the highest temperature at which the last trace of crystallinity

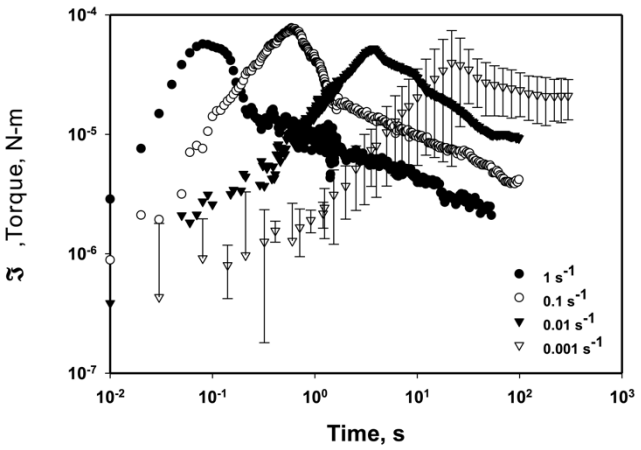

Figure 10. Torque, ℑ, versus time, t, during steady torsional flow of P3HT/$PC_{60}BM$ solutions (at equal concentrations of 25 mg/mL) in o-DCB for apparent shear rates of 1, 0.1, 0.01 and 0.001 s^{-1} at −5 °C.

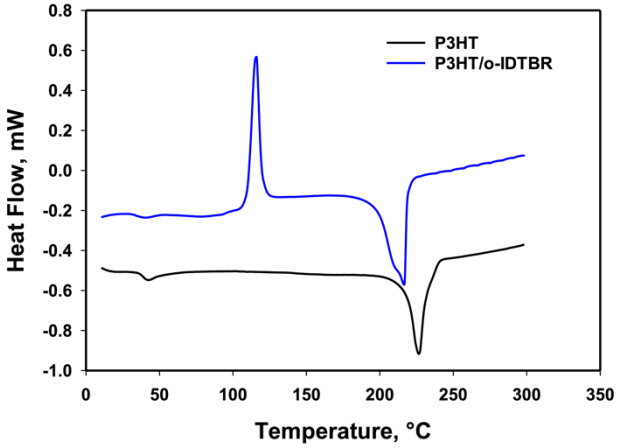

Figure 11. DSC second heating cycles of P3HT and 1:1 P3HT/o-IDTBR blend.

disappears (definition of the nominal melting temperature). Fig. 11 also shows the thermal behavior of P3HT. P3HT alone does not exhibit the crystallization behavior observed with the P3HT/o-IDTBR blend, i.e., the crystallization of P3HT occurs during the cooling stage. With the addition of o-IDTBR, crystallization continues during the heating stage and the temperatures for the onset of melting, the peak temperature and the melting temperature all shift to lower temperatures in comparison to those encountered for P3HT at the same heating rate. Overall, these results indicate that the crystallization of P3HT is disrupted by the mixing of the acceptor into P3HT.

For the P3HT samples that are obtained upon thermal treatment at −5 °C followed by solvent evaporation at the ambient temperature, the melting enthalpy (area under the peak) is about 10.1 J/g. Considering that the melting enthalpy of single crystals of P3HT (purely crystalline) is 99.0 J/g,[80] a degree of crystallinity of about 10.2% is obtained (by weight) indicating that the sample is mostly comprised of the amorphous phase. This emphasizes the importance of the presence of an amorphous phase during the crystallization of P3HT. The migration of the small acceptor molecules into the amorphous regions of P3HT can be substantial.[72]

We have also investigated the melting behavior of P3HT blended with $PC_{60}BM$ using differential scanning calorimetry. During the first heating of the dried P3HT and $PC_{60}BM$ blend film (equal concentrations of P3HT and $PC_{60}BM$) the first melting endotherm initiates at about 195 °C and is completed at 225 °C (results not shown). The second endotherm is observed to occur at about 289 °C and is completed at about 295 °C. For P3HT and $PC_{60}BM$ blends Lai et al. reported a first melting temperature of 220.2 °C and a second melting temperature of 284.6 °C. For pristine P3HT the melting temperature is 231.9 °C and for pristine $PC_{60}BM$ the melting temperature is 283.3 °C.[81] The relatively high temperatures necessary to melt the crystals of P3HT and small molecular acceptors (SMAs) indicate that the crystalline structures achieved due to low temperature exposure and shearing of the solutions would continue to partially prevail under processing at temperatures lower than the melting temperatures of the electron donor and acceptor components of the active layer (the amorphous components would relax). It was determined that there is a reduction of the crystallinity of P3HT when there is a small molecule acceptor present.[81] The SMAs act as an impurity that depresses the melting temperature of the semi-crystalline polymer.[82]

Chu et al. have shown that long range ordering and highly aligned P3HT thin films could be obtained by exposing the P3HT solution to UV-irradiation and solution aging followed by film deposition via blade coating method. The degree of chain alignment could be controlled by solution aging time. The shearing direction in blade coating further affected the charge transport anisotropies.[83] Our method of processing the P3HT solutions as gels at -5 °C and lower would generate the formation of aggregation and crystallization, some of which will be retained when the solution is brought back to the ambient temperature, presumably with the amorphous phase relaxing and some degree of crystalline order persisting.

Effects of the nanocrystalline structures achieved during exposures to low temperature or shearing under low temperatures to behavior when the temperature was returned to ambient were also investigated in our previous investigation.[58] For example, during temperature cycling while applying small-amplitude oscillatory shearing He et al., have shown that the maximum G′ could be achieved faster during the second time the temperature was reduced to -5 °C in comparison to the initial cooling.

What could be the thickness of the active layer from our P3HT solutions using for example a blade coating-based film formation method? Chu et al. 2016 have investigated the blade coating of P3HT solutions following aggregation and crystallization of P3HT as a result of exposure to ultraviolet radiation and aging of the P3HT solutions under ambient temperature conditions. The blade was vertical to the substrate at a fixed gap of 10 micronmeter. Considering that the P3HT concentration was 10 mg in 2 mL of solvent, the thickness of the dried active layer that they could achieve was about 45 nm (P3HT density of 1.1 g/cm^3 was assumed). Similar active layer thickness values can be expected from our P3HT solutions especially if pure drag flow based coating methods are utilized (the shear rate would be independent of the shear viscosity of the solutions/gel under pure drag flow conditions under controlled wall slip/stick conditions).[63]

Chu et al. 2016 also compared the charge mobility performance of the deposited and dried films with active layers deposited via spin coating at a spin speed of 1500 rpm for 60 s. The blade coated specimens gave rise to greater mobilities when the blade coating direction was in the direction that was vertical (transverse) with the source/drain electrodes.[83] Thus, mobilities commensurate with spin coating could be obtained from blade coated samples in spite of the viscosity increases associated with solution aging and UV exposure (unfortunately, no gelation studies nor rheological characterization results were available in these earlier investigations).

4 Conclusions

A major problem in the fabrication of bulk heterojunction based polymeric solar cells is the lack of a widely available continuous processing method. Generally, spin coating is used to lay a blend of an acceptor with a donor polymer as an active layer film, however, such coating is not scalable. One alternative would be the use of conventional fabrication methods including extrusion and coating of substrates to form the active layer continuously. However, the elasticity and the viscosity of typical acceptor/donor blends are too low to permit extrusion and coating processing under typically ambient conditions.

Here we have investigated the gelation of the donor/acceptor blends under sub-ambient conditions at which the blend forms a gel, to exhibit increases in elasticity and viscosity. The gelation dynamics and the associated rheological behavior were investigated for P3HT (regioregular) in conjunction with a non-fullerene acceptor, o-IDTBR and the results were compared with

those of P3HT/$PC_{60}BM$ blends. Solutions with two different solvents and with various donor/acceptor concentrations were prepared and subjected to sub-ambient conditions (−5 °C). The formation of strong gels of P3HT (as well as blends of P3HT with o-IDTBR) occurred at −5 °C. During the gelation process the dynamic properties increased to reach plateau values. Frequency sweeps were carried out after the plateau behavior was reached and revealed that the dynamic properties became independent of the frequency and that $G'>>G''$. Therefore, overall the energy dissipated as heat during oscillatory shearing, i.e., viscous dissipation represented by G'' was significantly smaller than the energy stored as elastic energy, as represented by G' (small of tan $\delta = G''/G'$ values) indicating gel-like behavior.

The time necessary to reach a stable gel structure decreased while the gel strength, i.e., the plateau values of the storage modulus, increased with the increasing concentration of P3HT. Furthermore, the increase of the gel strength of P3HT solutions at −5 °C was particularly significant when the concentration of P3HT increased from 12.5 mg/ml to 25 mg/ml (a jump from 800 to 10^4 Pa), whereas the gel strength values were relatively low (100-250 Pa) at concentrations which were smaller than 11 mg/ml and less.

The gel strengths of P3HT and P3HT blend solutions increased significantly for a good solvent (o-DCB) and decreased with a poor solvent (o-xylene). This can be linked to the expected increase of the radius of gyration of P3HT in the good solvent, rendering π-π interactions between P3HT macromolecules and hence aggregation more likely, thus increasing the crystallinity of P3HT, giving rise to increased gel strength. The incorporation of the non-fullerene acceptor o-IDTBR into P3HT again led to the formation of strong gels at −5 °C but the gel strength was reduced in comparison to that of P3HT blended with $PC_{60}BM$. The concentration of o-IDTBR did not make any difference on gel strength in the 25-50 mg/ml range at a P3HT concentration of 25 mg/ml. In comparison to the conventional P3HT/$PC_{60}BM$ system the gel strengths of P3HT/o-IDTBR blends are smaller, indicating that the crystalline network which forms during gelation is more pronounced for the P3HT/o-IDTBR system in comparison to P3HT/$PC_{60}BM$.

The time dependence of the steady torsional flows of the gels of P3HT and P3HT blends at −5 °C, suggests that shearing decreases the gel strength significantly (independent of the rheometer gap used). This significant dependence of the gel strength on the shearing history is indicative of the narrowness of the processability window of the gels of P3HT and P3HT blends. Shearing reduces the shear viscosity and the elasticity, i.e., the gel strength, of the gels, which form during sub-ambient processing. Overall, these results indicate that the gel structure is fragile in the non-linear viscoelastic range. This teaches that the rates of shear and elongation imposed during processing of P3HT and P3HT blend solutions in the gel state would play significant roles in the development of P3HT aggregates and nanowhisker networks and consequently the functional properties of the active layer. Thus, the structure of the gel during processing using conventional polymer processing equipment and the subsequent formation of the nanostructure of resulting bulk heterojunction devices, as well as their functional properties including PCEs, would all be interdependent. Our findings also indicate that the structure of the gel can be retained during processing if the imposed shear rates (and consequently strains) are relatively small. Processes with shear rate gradients across the film during processing (for example, Poiseuille flow) would result in structural heterogeneities across the film, likely deteriorating the functional properties of the active layer.

Conflicts of interest

There are no conflicts to declare.

Acknowledgements

This work was partially supported by funds from the National Science Foundation under Grant 1635284, the Highly Filled Materials Institute and by a gift from the PSEG Foundation to advance energy innovation at Stevens. We are grateful to our sponsors for making this investigation possible.

Supplemental files

Additional information on introduction to organic solar cells, differences between layered structures and heterogeneous bulk active layers, the crystallization of P3HT, the chemical structures of the electron acceptors, a typical twin screw extrusion process and coating unit that is applied during the fabrication of the active layer, the rheological characterization equipment and methods, and additional results related to time-dependent dynamic properties during gelation, steady torsional flow and differential scanning calorimetry of the first heating of the P3HT and P3HT blend solution with o_IDTBR are included in the supplemental file.

References

1 M. Jacoby, *Chem. Eng. News,* 2016, 94(18): 30-35.
2 D. Wöhrle and D. Meissner. *Advanced Materials,* 1991, 3(3): 129-138.
3 S. Günes, H. Neugebauer and N. S. Sariciftci. *Chemical reviews,* 2007, 107(4): 1324-1338.
4 N. S. Sariciftci, L. Smilowitz, A. J. Heeger and F. Wudl, *Science,* 1992, 258(5087): 1474-1476.
5 A. M. Bagher, M. M. A. Vahid and M. Mohsen. *American Journal of optics and Photonics,* 2015, 3(5): 94-113.
6 A. Gusain, R. Faria and P. Miranda, *Frontiers in chemistry*, 2019, 7: 61.
7 C. J. Brabec, N. S. Sariciftci and J. C. Hummelen, *Advanced functional materials,* 2001, 11(1): 15-26.
8 E. Bundgaard and F. C. Krebs, *Solar Energy Materials and Solar Cells,* 2007, 91(11): 954-985.
9 D. Chen, A. Nakahara, D. Wei, D. Nordlund, and T. P. Russell, *Nano letters,* 2011, 11(2): 561-567.

10 M. Jørgensen, K. Norrman and S. A. Gevorgyan, T. Tromholt, B. Andreasen and F. C. Krebs, *Advanced materials,* 2012, 24(5): 580-612.
11 S. Holliday, R. S. Ashraf, A. Wadsworth, D. Baran, S. A. Yousaf, C. B. Nielsen, C. H. Tan, S. D. Dimitrov, Z. Shang, N. Gasparini, M. Alamoudi, F. Laquai, C. J. Brabec, A. Salleo, J. R. Durrant and I. McCulloch, *Nature communications,* 2016, 7: 11585.
12 C. J. Mulligan, M. Wilson, G. Bryant, B. Vaughan, X. Zhou, W. J. Belcher, P. C. Dastoor, *Solar Energy Materials and Solar Cells,* 2014, 120: 9-17.
13 R. Po, A. Bernardi, A. Calabrese, C. Carbonera, G. Corsoa and A. Pellegrinoa, *Energy & Environmental Science,* 2014, 7(3): 925-943.
14 K. Tremel and S. Ludwigs, *Springer Berlin Heidelberg,* 2014.
15 M. Giulianini and N. Motta. *Springer,* New York, NY, 2012: 1-72.
16 M. A. Ansari, S. Mohiuddin, F. Kandemirli and M. I. Malik, *RSC advances,* 2018, 8(15): 8319-8328.
17 M. Naito, K. Nobusawa, H. Onouchi, Masashi Nakamura, K. Yasui, A. Ikeda and M. Fujiki, *Journal of the American Chemical Society,* 2008, 130(49): 16697-16703.
18 W. Yi, A. Malkovskiy and Q. Chu, A. P. Sokolov, M. L. Colon, M. Meador and Y. Pang, *The Journal of Physical Chemistry B,* 2008, 112(39): 12263-12269.
19 J. H. Bannock, S. H. Krishnadasan, A. M. Nightingale, C. P. Yau, K. Khaw, D. Burkitt, J. J. M. Halls, M. Heeney, J. C. de Mello, *Advanced Functional Materials,* 2013, 23(17): 2123-2129.
20 M. Bernardi, M. Giulianini and J C. Grossman. *ACS nano,* 2010, 4(11): 6599-6606.
21 M. Aryal, K. Trivedi and W. Hu. *ACS nano,* 2009, 3(10): 3085-3090.
22 J. Xiao, J. Shi, H. Liu, Y. Xu, S. Lv, Y. Luo, D. Li, Q. Meng, Y. Li, *Advanced Energy Materials,* 2015, 5(8): 1401943.
23 V. Skrypnychuk, N. Boulanger, V. Yu, M. Hilke, S. C. B. Mannsfeld, M. F. Toney, D. R. Barbero, *Advanced Functional Materials,* 2015, 25(5): 664-670.
24 M. Giulianini and N. Motta, *Self-Assembly of Nanostructures. Springer, New York, NY,* 2012: 1-72.
25 Y. Sun, Y. C. Han and J. G. Liu. *Chinese Science Bulletin,* 2013, 58(22): 2767-2774.
26 N. Espinosa, M. Hösel, M. Jørgensen and F. C. Krebs, *Energy & Environmental Science,* 2014, 7(3): 855-866.
27 L. Persano, A. Camposeo and D. Pisignano, *Progress in polymer science,* 2015, 43: 48-95.
28 N. S. Sariciftci, D. Braun, C. Zhang, V. I. Srdanov, A. J. Heeger, G. Stucky and F. Wudl, *Applied physics letters,* 1993, 62(6): 585-587.
29 M. M. Wienk, J. M. Kroon, W. J. H. Verhees, J. Knol, J. C. Hummelen, P. A. van Hal, R. A. J. Janssen, *Angewandte Chemie,* 2003, 115(29): 3493-3497.
30 B. M. Savoie, K L. Kohlstedt, N E. Jackson, L. X. Chen, M. O. de la Cruz, G. C. Schatz, T. J. Marks and M. A. Ratner, *Proceedings of the National Academy of Sciences,* 2014, 111(28): 10055-10060.
31 E. Kozma, M. Catellani. *Dyes and Pigments,* 2013, 98(1): 160-179.
32 A. J. Moule, D. Neher and S. T. Turner, *P3HT Revisited–From Molecular Scale to Solar Cell Devices. Springer, Berlin, Heidelberg,* 2014: 181-232.
33 S. E. Shaheen, C. J. Brabec, N. S. Sariciftci, F. Padinger, T. Fromherz and J. C. Hummelen, *Applied Physics Letters,* 2001, 78(6): 841-843.
34 F. Padinger, R. S. Rittberger and N. S. Sariciftci, *Advanced Functional Materials,* 2003, 13(1): 85-88.
35 G. Li, V. Shrotriya, Y. Yao and Y. Yang, *Journal of Applied Physics,* 2005, 98(4): 043704.
36 W. Ma, C. Yang, X. Gong, K. Lee and A. J. Heeger, *Advanced functional materials,* 2005, 15(10): 1617-1622.
37 D. M. González, V. Körstgens, Y. Yao, L. Song, G. Santoro, S. V. Roth and P. Müller-Buschbaum, *Advanced Energy Materials,* 2015, 5(8): 1401770.
38 J. Yuan, Y. Zhang, L. Zhou, G. Zhang, H. Yip, T. K. Lau, X. Lu, C. Zhu, H. Peng, P. A. Johnson, M. Leclerc, Y. Cao, J. Ulanski, Y. Li and Y. Zou, *Joule,* 2019, 3(4): 1140-1151.
39 Y. Lin, J. Wang, Z. G. Zhang, H. Bai, Y. Li, D. Zhu and X. Zhan, *Advanced materials,* 2015, 27(7): 1170-1174.
40 N. Gasparini, M. Salvador, S. Strohm, T. Heumueller, I. Levchuk, A, Wadsworth, J. H. Bannock, J. C. de Mello, H. J. Egelhaaf, D. Baran, I. McCulloch and C. J. Brabec, *Advanced Energy Materials,* 2017, 7(19): 1700770.
41 D. Baran, R. S. Ashraf, D. A. Hanifi, M. Abdelsamie, N. Gasparini, J. A. Röhr, S. Holliday, A. Wadsworth, S. Lockett, M. Neophytou, C. J. M. Emmott, J. Nelson, C. J. Brabec, A. Amassian, A. Salleo, T. Kirchartz, J. R. Durrant and I. McCulloch, *Nature materials,* 2017, 16(3): 363-369.
42 S. F. Hoefler, T. Rath, N. Pastukhova, E. Pavlica, D. Scheunemann, S. Wilken, B. Kunert, R. Resel, M. Hobisch, S. Xiao, G. Bratina and G. Trimmel, *Journal of Materials Chemistry A,* 2018, 6(20): 9506-9516.
43 C. H. Tan, A. Wadsworth, N. Gasparini, S. Wheeler, S. Holliday, R. S. Ashraf, S. D. Dimitrov, D. Baran, I. McCulloch and J. R. Durrant, *The Journal of Physical Chemistry C,* 2018, 123(10): 5826-5832.
44 Q. Liang, X. Jiao, Y. Yan, Z. Xie, G. Lu, J. Liu and Y. Han, *Advanced Functional Materials,* 2019, 29(47): 1807591.
45 J. I. Khan, R S. Ashraf, M A. Alamoudi, M. N. Nabi, H. N. Mohammed, A. Wadsworth, Y. Firdaus, W. Zhang, T. D. Anthopoulos, I. McCulloch and F. Laquai, *Solar RRL,* 2019, 3(8): 1900023.
46 E. Pascual-San-José, X. Rodríguez-Martínez, R. Adel-Abdelaleim, M. Stella, E. Martínez-Ferrero and M. Campoy-Quiles, *Journal of Materials Chemistry A,* 2019, 7(35): 20369-20382.
47 J. Liu, S. Zeng, P. Jing, K. Zhao and Q. Liang, *Journal of Energy Chemistry,* 2020, 52, 333-341.
48 K. An, W. Zhong and L. Ying, *Organic Electronics,* 2020: 105701.
49 F. C. Krebs, *Solar energy materials and solar cells,* 2009, 93(4): 394-412.
50 D. M. Kalyon, D. Dalwadi, M. Erol, E. Birinci and C. Tsenoglou, *Rheologica acta,* 2006, 45(5): 641-658.

51 M. Erol and D. M. Kalyon, *International Polymer Processing,* 2005, 20(3): 228-237.
52 R. Yazici and D. M. Kalyon, *Rubber chemistry and technology,* 1993, 66(4): 527-537.
53 A. Lawal and D. M. Kalyon, *Journal of Applied Polymer Science,* 1995, 58, 1501-1507.
54 D. M. Kalyon and M. Malik, *International Polymer Processing,* 2007, 22(3): 293-302.
55 M. Malik and D. Kalyon, *International Polymer Processing,* 2005, 20(4): 398-409.
56 M. Malik, D. M. Kalyon, and J. C. Golba Jr., *International Polymer Processing,* 2014, 29(1): 51-62.
57 D. M. Kalyon, H. Gevgilili and A. Shah, *International Polymer Processing,* 2004, 19(2): 129-138.
58 J. He, X. Kong, Y. Wang, M. Delaney, D. M. Kalyon and S. S. Lee, *ACS Applied Polymer Materials,* 2019, 1(3): 500-508.
59 H. Tanaka, *Journal of Physics: Condensed Matter,* 2000, 12(15): R207.
60 H. Tanaka and T. Araki*, Chemical engineering science,* 2006, 61(7): 2108-2141.
61 H. Tanaka, *Advanced Materials,* 2009, 21(18): 1872-1880.
62 B. K. Aral and D. M. Kalyon. *Journal of Rheology,* 1994, 38(4): 957-972.
63 D. M. Kalyon. *Journal of Rheology,* 2005, 49(3): 621-640.
64 S. Aktas, D. M. Kalyon and B. M. Marín-Santibáñez and J. Pérez-González, *Journal of Rheology,* 2014, 58(2): 513-535.
65 J. F. Ortega-Avila, J. Pérez-González, B M. Marín-Santibáñez, F. Rodríguez-González, S. Aktas, M. Malik and D. M. Kalyon, *Journal of Rheology,* 2016, 60(3): 503-515.
66 E. F. Medina-Bañuelos, B M. Marín-Santibáñez and J. Pérez-González, M. Malik and D. M. Kalyon, *Journal of Rheology,* 2017, 61(5): 1007-1022.
67 H. H. Winter and F. Chambon. *Journal of rheology,* 1986, 30(2): 367-382.
68 J. Liu, M. Arif, J. Zou, S. I. Khondaker and L. Zhai, *Macromolecules,* 2009, 42(24): 9390-9393.
69 F. Machui, S. Langner, X. Zhu, S. Abbott and C. J. Brabec, *Solar Energy Materials and Solar Cells,* 2012, 100: 138-146.
70 S. Lee, H. Jeon, M. Jang, K. Y. Baek and H. Yang, *ACS applied materials & interfaces,* 2015, 7(2): 1290-1297.
71 J. Luke, E. M. Speller, A. Wadsworth, M. F. Wyatt, S. Dimitrov, H. K. H. Lee, Z. Li, W. C. Tsoi, I. McCulloch, D. Bagnis, J. R. Durrant and J. S. Kim, *Advanced Energy Materials,* 2019, 9(15): 1803755.
72 B. A. Collins, E. Gann, L. Guignard, X. He, C. R. McNeill and H. Ade, *The Journal of Physical Chemistry Letters,* 2010, 1(21): 3160-3166.
73 E. F. Medina-Bañuelos, B M. Marín-Santibáñez and J. Pérez-González and D. M. Kalyon, *Journal of Rheology,* 2019, 63(6): 905-915.
74 H. Gevgilili and D M. Kalyon, *Journal of Rheology,* 2001, 45(2): 467-475.
75 D. M. Kalyon and H. Gevgilili, *Journal of Rheology,* 2003, 47(3): 683-699.
76 E. Birinci and D. M. Kalyon, *Journal of Rheology,* 2006, 50(3): 313-326.
77 H. S. Tang and D M. Kalyon, *Journal of Rheology,* 2008, 52(2): 507-525.
78 H. S. Tang and D M. Kalyon, *Journal of Rheology,* 2008, 52(5): 1069-1090.
79 D. M. Kalyon and S. Aktas, *Annual review of chemical and biomolecular engineering,* 2014, 5: 229-254.
80 J. Zhao, A. Swinnen, G. Van Assche, J. Manca, D. Vanderzande and B. V. Mele, *The Journal of Physical Chemistry B,* 2009, 113(6): 1587-1591.
81 Y. C. Lai, T. Higashihara, J. C. Hsu, M. Uedab and W. C. Chen, *Solar energy materials and solar cells,* 2012, 97: 164-170.
82 G. F. Malgas, D. E. Motaung and C. J. Arendse, *Journal of Materials Science, 2012,* 47(10): 4282-4289.
83 P. H. Chu, N. Kleinhenz, N. Persson, M. McBride, J. L. Hernandez, B. Fu, G. Zhang and E. Reichmanis, *Chemistry of Materials*, 2016, 28(24): 9099-9109.